DOI: 10.13009/EUCASS2019-967

A diffusion model in velocity space to describe the electron dynamics in an ECR plasma thruster with magnetic nozzle

Simon Peterschmitt, Jean C. Porto **, Paul-Quentin Elias***, Denis Packan*****
DPHY, ONERA, Université Paris Saclay
F-91123 Palaiseau – France
** simon.peterschmitt@onera.fr*
*** jean_carlos.porto_hernandez@onera.fr*
**** paul-quentin.elias@onera.fr*
***** denis.packan@onera.fr*

Abstract

A quasi-linear heating model for an electron cyclotron resonance acceleration (ECR) thruster is presented. It consists of a Fokker-Planck equation in perpendicular velocity, with a loss term accounting for the deconfinement of electrons from the magnetic field. It is a global model in space that calculates an electron perpendicular velocity distribution function resulting from several passes through the electron cyclotron resonance region. The results are interpreted to provide an estimate of the plasma flow in the jet as well as the accelerating potential. A simple parametric study is presented as well as a preliminary comparison with experimental data.

Nomenclature

ECR = Electron Cyclotron Resonance
PIC = Particle-In-Cell
SEE = Secondary Electron Emission
sccm = Standard cubic centimetre per minute
μ = Magnetic moment
ϕ = Electrostatic potential
B = Static magnetic field
τ_B = Bounce period
D = Diffusion coefficient
P = Distribution function in perpendicular velocity in the interaction region
$v_\perp$ = Perpendicular velocity in the interaction region
F_0 = Electron flux entering the system at low energy
F_* = Electron flux in the jet, exiting the system at high energy
v_0 = Velocity of low energy electrons entering the system
v_* = Velocity of electrons exiting the system at high energy
L_{el} = Integrated number of elastic collisions per unit time
L_i = Integrated number of ionizing collisions per unit time
K = Integrated power loss due to collisions
ψ_g = Neutral gas flow
P_{in} = Microwave input power
γ = Secondary electron emission yield on the “backplate”

DOI: 10.13009/EUCASS2019-967

1 Introduction

Small satellite launches have recently been increasing and are expected to surge in the next decade. Micro-propulsion has been identified has one of the major technological challenges for the development of small satellites [1]. Miniaturization of existing technologies as well as innovative concepts have been proposed. The Electron Cyclotron Resonance (ECR) thruster currently under development in the framework of the MINOTOR project [2] appears as a potentially disruptive technology on this market. This concept could lead to a robust, easy to operate, and low cost propulsion system.

Both experimental [3], [4] and PIC simulation [5] efforts are conducted at ONERA in order to understand the physics at play in the ECR thruster. The model presented in this paper is inspired from the current output of that work. It does not aim at describing the detailed dynamics of the magnetic nozzle as is done in [6], but rather is an attempt to encapsulate under a simple analytical formulation, some of the relevant physical phenomena regarding electron dynamics in the system formed by the coupled ionization source and magnetic nozzle. It focuses on the formation of the energy distribution of the population described in [7] as "trapped electrons", taking into account a model for the resonant heating process.

In the next paragraphs of section 1, an implementation of the ECR thruster currently under development at ONERA will be presented. Section 2 will lay out the main ideas of the model, present the key phenomena that are considered and state the equations of the model. In section 3, current results and a preliminary comparison with experimental data will be presented.

Figure 1 is a schematic view of a typical implementation of the thruster. It consists of a 27.5 mm diameter and 15 mm long semi-open coaxial coupling structure. Xenon gas is injected at a typical massflow of 1sccm and typically 30 W of microwave power at 2.45 GHz are fed through a boron nitride "backplate" at the close end of the coaxial structure. It is immersed in a static and divergent magnetic field that is created by an annular permanent magnet.

The electrons are assumed to be resonantly coupled to the microwave field in the vicinity of the ECR surface where the magnetic field is such that the gyro-frequency of the electrons ($\omega_{ce} = qB/m$) equals the frequency of the wave (B = 875G for f = 2.45 GHz). The required power for heating and ionizing is deposited in the plasma of electrons through this interaction. The electron dynamics in the diverging magnetic field then establishes an axial potential drop of typically 200 eV, accelerating the ions out of the thruster.

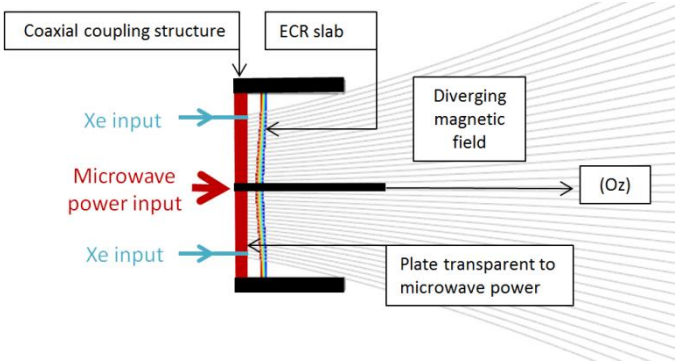

Figure 1 : Schematic of a typical implementation of the coaxial ECR thruster

2 Presentation of the model

DOI: 10.13009/EUCASS2019-967

2.1 Pseudo-periodic motion

The model is a global description on the magnetic tube going through the open end section of the thruster (Figure 1). Two separate idealized regions are considered. The first region, thereafter named the interaction region, is a the section of the coaxial chamber containing the ECR slab near the closed end of the source where electrons interact both with relatively dense neutral gas and with relatively intense microwave field.

In a second region extending to the right (the plume), the electrons are distant from the heating zone and it is assumed that their guiding centres follow trajectories along the field lines, governed only by the diamagnetic and the electrostatic force. The equation of motion along the axis of symmetry (Oz as showed in Figure 1) is simply

$$m\frac{dv_z}{dt} = -\mu\frac{\partial B_z}{\partial z} + e\frac{\partial \phi}{\partial z} \quad (1)$$

where m is the electron mass, $\mu = mv_\perp^2/(2B)$ is the magnetic moment, e is the absolute value of the elementary charge and ϕ the electrostatic potential. μ is a constant of the motion provided that the spatial variation of the magnetic field B inside the electron orbit is small compared to its magnitude [8].

Based on the static magnetic field B that is imposed by the magnet, as well as measurements of the electrostatic potential [9] made on the thruster, the typical axial shape of the fields is shown in Figure 2. Electrons created in the thruster oscillate in the effective potential $U_{eff} = \mu B - e\phi$ with a period usually referred to as the bounce time τ_B. On the left side they are confined by the converging magnetic field lines as well as the electrostatic potential of the sheath formed at the backplate. On the right side they are confined by the electrostatic field only.

If B is linearized as $B = B_0(1 - \alpha z)$ and ϕ is assumed to have a concave quadratic shape $\phi = -\phi_0 z^2$ then equation (**1**) is the equation for an harmonic oscillator of period:

$$\tau_B = \frac{2\pi}{\sqrt{\frac{2e\phi_0}{m}}} \quad (2)$$

The motion is called pseudo-periodic in that, additionally to the periodic “bounce motion”, electrons can undergo interaction with the neutral gas and the microwave field at each period, when they go through the interaction region.

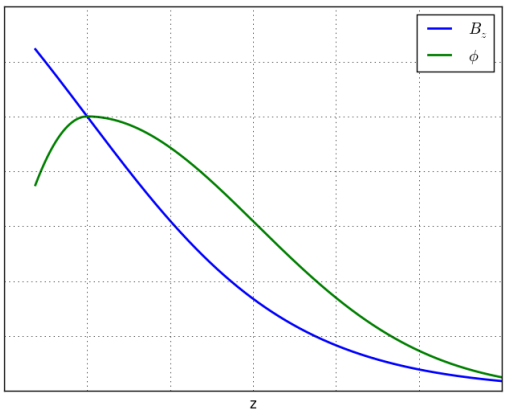

Figure 2 : Normalized typical shape of magnetic field and electrostatic potential

DOI: 10.13009/EUCASS2019-967

2.2 Confinement

Electrons are assumed to follow the magnetic field lines unless they undergo a collision. The energy of the microwave is assumed to be deposited in the perpendicular kinetic energy of the electrons (that is, in μ). Therefore, electrons stay confined on the left as they gain perpendicular energy in the resonance layer (Figure 3). After sufficient energy gain they can overcome the electrostatic potential barrier and leave the thruster potential well to the right side, therefore contributing to thrust. This situation can be represented in velocity space by a confinement figure at a given axial location. Inside this figure, are confined $(v_{\parallel}, v_{\perp})$ pairs.

Among the different deconfinement mechanisms (electron demagnetization, turbulent cross field diffusion), elastic and ionisation collisions with neutral gas are assumed to be dominant. A collision is modelled by a random scattering of the electron velocity vector on a circle of appropriate kinetic energy in the $(v_{\parallel}, v_{\perp})$ plane. For elastic collisions, where the kinetic energy is conserved, the equation below shows the relationship between the pre- and post-collision velocities (primed variables). This is the equation of a centred circle.

$$v_{\perp}^2 + v_{\parallel}^2 = v_{\perp}'^2 + v_{\parallel}'^2 \qquad (3)$$

In the thruster, the gas is injected at the backplate. Due to the rapid gas expansion in vacuum, electrons are assumed to interact with neutrals only in the interaction region, close to the backplate. In this region, the confinement surface is very narrow (Figure 4) thus the random redistribution of the electron on a circle of appropriate kinetic energy is most likely to extract it from the confinement surface. Therefore, as a first approximation, any collision is considered as deconfining the electron. It results in an impact on the backplate and possibly emission of a secondary electron.

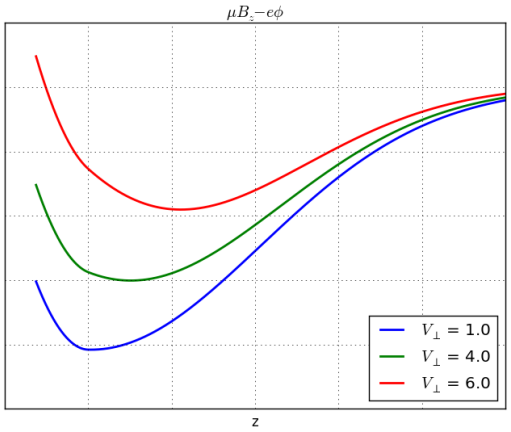

Figure 3 : Confining potentials corresponding to the fields of Figure 2 for several perpendicular velocities in arbitrary units

DOI: 10.13009/EUCASS2019-967

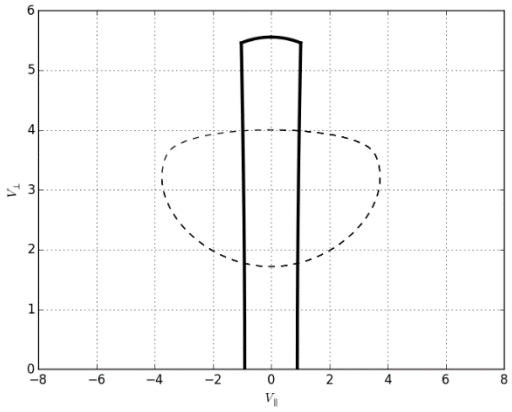

Figure 4 : Solid line: typical shape of the confinement zone at the axial location of the interaction region. An electron crossing the upper boundary as acquired enough kinetic energy to overcome the electrostatic barrier and can leave the thruster in the jet. Electrons are crossing the side boundary as the result of collisions and are collected at the backplate. Dashed line: periodic electron orbit in the fields of Figure 2. Arbitrary units.

2.3 Heating

To model the heating process, a Boltzmann equation is considered [10]. It is assumed that the only relevant parameter is the perpendicular velocity in the interaction region $v_\perp$ and that the phase difference between the cyclotron motion and the phase of the microwave electric field at resonance bear no correlation between two successive passes. If $P(v_\perp, t)$ is a distribution function and w is a transition rate modelling the change in velocity for a single pass in the resonant region:

$$\frac{\partial P(v_\perp,t)}{\partial t} = \int [w(v_\perp \leftarrow v_\perp + \widetilde{v_\perp})\, P(v_\perp + \widetilde{v_\perp}, t) - w(v_\perp + \widetilde{v_\perp} \leftarrow v_\perp)\, P(v_\perp, t)] d\widetilde{v_\perp} \quad (4)$$

Under the assumption that the velocity increment is small, that is $\widetilde{v_\perp} \longmapsto w(v_\perp \leftarrow v_\perp + \widetilde{v_\perp})$ is a narrow function compared to the distribution function, a Fokker-Planck equation can be derived from equation (4)

$$\frac{\partial P(v_\perp,t)}{\partial t} = -\frac{\partial}{\partial v_\perp}\left[\frac{\langle \delta\widetilde{v_\perp}\rangle}{\delta t} P(v_\perp,t) - \frac{\partial}{\partial v_\perp}\left(\frac{\langle \delta\widetilde{v_\perp}\delta\widetilde{v_\perp}\rangle}{2\delta t} P(v_\perp,t)\right)\right] \quad (5)$$

where $\langle \delta\widetilde{v_\perp}\rangle/\delta t$ and $\langle \delta\widetilde{v_\perp}\delta\widetilde{v_\perp}\rangle/\delta t$ are first and second order moments of the transition rate. Since the resonant absorption of electromagnetic wave by an electron can be considered a reversible process, that is $w(v_\perp + \widetilde{v_\perp} \leftarrow v_\perp) = w(v_\perp \leftarrow v_\perp + \widetilde{v_\perp})$, equation (5) can take the so called quasi-linear form [10] :

$$\frac{\partial P(v_\perp,t)}{\partial t} = \frac{\partial}{\partial v_\perp}\left[\frac{\langle \delta\widetilde{v_\perp}\delta\widetilde{v_\perp}\rangle}{2\delta t} \frac{\partial P(v_\perp,t)}{\partial v_\perp}\right] \quad (6)$$

An additional loss term is inserted in this equation to account for collisions. Collisions are not modelled with a friction term but rather in an idealised way: any collision is assumed to deconfine the particle therefore collisions are treated as a plain loss. Moreover $\langle \delta\widetilde{v_\perp}\delta\widetilde{v_\perp}\rangle/(2\delta t)$ is thereafter noted as a diffusion coefficient $D(v_\perp)$ for simplification, and also to emphasize that the heating process can be understood as a diffusion in velocity space. Equation 5 can then be recast as:

DOI: 10.13009/EUCASS2019-967

$$\frac{\partial P(v_\perp,t)}{\partial t} = \frac{\partial}{\partial v_\perp}\left[D(v_\perp)\ \frac{\partial P(v_\perp,t)}{\partial v_\perp}\right] - \left(\frac{1}{\tau_{el}} + \frac{1}{\tau_i}\right) P(v_\perp,t) \quad (7)$$

with

$$\frac{1}{\tau_{el}} = \sigma_{el} n_g v_\perp \qquad \frac{1}{\tau_i} = \sigma_i n_g v_\perp \quad (8)$$

where n_g is the neutral gas density, σ_{el} and σ_i are the elastic and ionization cross sections.

The choice of the coefficient $D(v_\perp)$ of this Fokker-Planck equation is a very important and delicate issue. As a first step it is written as

$$D(v_\perp) = \frac{\Delta V^2}{2\tau_B} \quad (9)$$

ΔV representing the root mean square of the statistical change in velocity for one pass in the resonant region. ΔV is taken from [11] as

$$\Delta V = 0.71\ \frac{e}{m} E\ \omega^{-1} \left(\frac{2\omega}{\alpha v_\perp}\right)^{2/3} \quad (10)$$

where E is the norm of the electric field at resonance α the scale length of variation of B and ω the frequency of the wave.

2.4 Particle balance equation – boundary conditions

The velocity spread of the distribution function P is bounded at low energy by v_0 which is the mean energy of the electrons produced by secondary electron emission and ionization events in the interaction region. These electrons are supposed to have a velocity of a few eV [12]. Electrons which have gained enough kinetic energy will leave the potential well when $v_\perp \geq v_*$. Above that value P is zero.

The total number of electrons is $N = \int_{v_0}^{v_*} P(v_\perp,t) dv_\perp$. Thus, equation (7) can be integrated to get the particle balance:

$$\frac{dN}{dt} = F_* + F_0 - L_{el} - L_i \quad (11)$$

Here, F_* is the particle flux lost in the jet. Since the thruster does not collect electrons but on the contrary expels a quasi-neutral plasma, one has that $F_* \leq 0$, meaning that electrons are lost in the jet. By definition L_{el} and L_i, the loss terms due to elastic collisions and ionization, are positive.

$$L_i = \int \frac{P(v_\perp,t)}{\tau_i} dv_\perp \qquad L_{el} = \int \frac{P(v_\perp,t)}{\tau_{el}} dv_\perp \quad (12)$$

If the only creation term of low energy electrons is the ionization, then $F_0 = L_i$ and the balance equation is $\frac{dN}{dt} < 0$, meaning that no steady state can be reached. One see that an additional creation mechanism of electrons at low energy is required to sustain a steady regime.

Accounting for secondary electron emission on the backplate (see section 2.2), one can consider that

$$F_0 = L_i + \gamma(L_i + L_{el}) \tag{13}$$

Under this condition, a steady regime is possible and we have at steady state

$$F_* + (\gamma - 1)L_{el} + \gamma L_i = 0 \tag{14}$$

This means that the flux of electrons in the jet is related to the production of secondary electrons at the backplate.

2.5 Energy balance equation

An energy balance equation is derived from equation (7). Multiplying by the kinetic energy and integrating by parts yields

$$\begin{aligned}\int \frac{\partial P(v_\perp,t)}{\partial t}\frac{1}{2}m\,{v_\perp}^2\,dv_\perp \\ = \left[D(v_\perp)\frac{\partial P(v_\perp,t)}{\partial v_\perp}\frac{1}{2}m\,{v_\perp}^2\right]_{v_0}^{v_*} - \int_{v_0}^{v_*} D(v_\perp)\frac{\partial P(v_\perp,t)}{\partial v_\perp}m\,v_\perp dv_\perp \\ - \int_{v_0}^{v_*}\left(\frac{1}{\tau_{el}}+\frac{1}{\tau_i}\right)P(v_\perp,t)\frac{1}{2}m\,{v_\perp}^2\,dv_\perp\end{aligned} \tag{15}$$

where v_* is the velocity above which electrons are lost in the jet and v_0 is the mean velocity of electrons created at low energy by ionization and secondary electron emission. The first term on the right hand side accounts for the energy flux related to those electrons. The second term is a heating term that is identified as the microwave power input in the system.

$$P_{in} = -\int_{v_0}^{v_*} D(v_\perp)\frac{\partial P(v_\perp,t)}{\partial v_\perp}m\,v_\perp dv_\perp \tag{16}$$

The third term accounts for the power lost because of collisions. Under the assumptions of this model, this power is deposited at the backplate. Let us define

$$K = \int_{v_0}^{v_*}\left(\frac{1}{\tau_{el}}+\frac{1}{\tau_i}\right)P(v_\perp,t)\frac{1}{2}m\,{v_\perp}^2\,dv_\perp \tag{17}$$

2.6 Neutral gas depletion

A balance equation for neutral gas density n_g is considered, including a source term for the gas inlet ψ_g, a loss term $V_{th}\,S\,n_g$ accounting for gas escaping to the right from the interaction region and two integral loss terms accounting for collisions. The density of gas is assumed to be zero outside of the interaction region and have a constant value inside.

$$\frac{\partial n_g}{\partial t} = \psi_g - V_{th}\,S\,n_g - \gamma\,L_i + (1-\gamma)L_{el} \tag{18}$$

The coefficients multiplying L_i and L_{el} factor the recombination and secondary electron emission at the backplate, which are subsequent to any collision (see section 2.2). An ionization event immediately implies the loss of a neutral but also the gain of a neutral (recombination at the backplate) and the loss of γ neutrals (to balance SEE at the

DOI: 10.13009/EUCASS2019-967

backplate). An elastic collision event implies the gain of a neutral (recombination at the backplate) and the loss of γ neutrals (SEE at the backplate).

2.7 Equations to be solved

The steady state equations are considered. The ordinary differential equation (7) is solved iteratively for the distribution function in perpendicular velocity in the interaction region $P(v_\perp)$, under the constraints imposed by integral equations (13), (15) and (18). The equations to be solved are recast as the following system (19):

$$\begin{aligned} &\frac{\partial}{\partial v_\perp}\left[D(v_\perp)\,\frac{\partial P(v_\perp,t)}{\partial v_\perp}\right]-\left(\frac{1}{\tau_{el}}+\frac{1}{\tau_i}\right)P(v_\perp,t)=0 \\ &F_0=\ -D(v_\perp)\frac{\partial P(v_\perp)}{\partial v_\perp}\bigg|_{v_0}\ =\ (1+\gamma)\,L_i\ +\ \gamma\,L_{el} \\ &\psi_g=\ V_{th}\,S\,n_g+\ \gamma\,L_i-\ (1-\gamma)L_{el} \\ &P_{in}=K-\ F_*\frac{1}{2}m\,{v_*}^2-F_0\frac{1}{2}m\,{v_0}^2 \end{aligned} \qquad (19)$$

The input parameters to be set are P_{in} , ψ_g, γ and the function $D(v_\perp)$. Tables for and $\sigma_{el}(v)$ and $\sigma_i(v)$ should be provided.

3 Results

3.1 Choice of input parameters in interpretation of the results

The main parameters to be set for each run of the model are the input power P_{in}, the xenon flow rate ψ_g, and the secondary electron emission coefficient at the backplate γ. For simplicity γ is modelled as an integrated constant value over incident energy. For a boron nitride backplate, as is commonly used in experiments, values between 1.4 and 2.0 are reasonable [12]. The input power typically ranges between 10 and 50 W and the xenon mass flow rate is typically between 0.06 and 0.4 mg/s. In addition, ionization and elastic cross section for xenon are taken from [13].

Besides, in order to set the diffusion coefficient $D(v_\perp)=\Delta V(v_\perp,E)^2/2\tau_B$, an estimate of the norm of the microwave electric field E in the interaction region has to be assumed, along with a value for the bounce period τ_B. The bounce period τ_B is taken as in equation (2). E is taken to be the average value $\bar{E}$ over the section of the coaxial coupling structure of the thruster (see Figure 1), of the norm of the electric field of the TEM mode of the coaxial line. If R_2 and R_1 are the diameters of the outer and inner conductor respectively, straightforward analytical calculation provides a relation between $\bar{E}$ and the power flowing in the coaxial line, identified to P_{in}:

$$\mathrm{P}_{in}=\frac{1}{4}\sqrt{\frac{\epsilon_0}{\mu_0}}\pi\ln\left(\frac{R_2}{R_1}\right)(R_2+R_1)^2\bar{E}^2=1.14\ 10^{-6}\,\bar{E}^2 \qquad (20)$$

A typical curve of $P(v_\perp)$ is shown on Figure 5. This curve is interpreted as the electron distribution function in perpendicular velocity in the interaction region, spatially integrated over the full thruster and plotted against energy in the interaction region, where the parallel energy is negligible.

The energy for which the curves reaches zero is interpreted as the energy of electrons exiting the thruster through the jet. Far enough from the thruster, where the magnetic and electrostatic field reach their zero asymptotic values, this energy is fully converted to parallel energy. If we equate the energy of an electron ion pair before and after exiting the thruster we get

$$\frac{1}{2}mv_* = \frac{1}{2}mv_{\parallel} + \frac{1}{2}MV_i \qquad (21)$$

where m and M, $v_{\parallel}$ and V_i , are the mass and average parallel velocity in the jet for electrons and ions respectively. Since the thruster is at floating potential, the ion flux (mainly constituted of singly charged ions) equals the electron flux in permanent regime. Besides, where the fields reach their asymptotic values, the plasma is still at a density where quasi neutrality is required, implying that the average electron and ion velocities are the same: $v_{\parallel} = V_i$. Since $m \ll M$, we get that the electron energy is almost fully transferred to ions. This transfer is achieved through the establishment of an ambipolar potential. The energy for which the curve in Figure 5 reaches zero is therefore interpreted as the ion energy.

The slope of the curve at the point where it reaches zero is the flux of electrons exiting the thruster through the jet. Since the thruster is at a floating potential, it is interpreted as an ion flux.

The model therefore provides a value for ion energy and ion flow. The dynamics in the magnetic nozzle being at least a 2 dimensional problem in space, this model cannot provide an angular ion flow profile. Therefore, in order to calculate thrust, some angular ion flow profile (or divergence efficiency) has to be assumed.

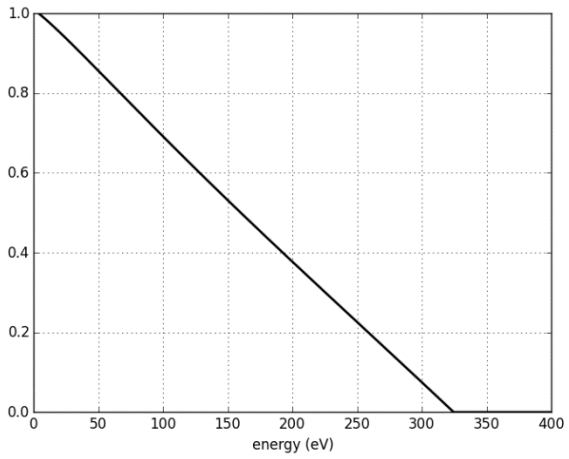

Figure 5 : Distribution of perpendicular velocity in the interaction region for P_{in} = 20 W, ψ_g= 0.1 mg/s, γ = 1.8

In the case of Figure 5 the ion energy is 325 eV and the ion flow is 0.77 of the input neutral gas flow which are values in the range of what can be measured experimentally for the ECR thruster.

3.2 Preliminary comparison with experimental data

Results for several sets of parameters are shown on Table 1. The ion energy and the ion mass flow (as fraction of the input gas flow) are increasing with input power and decreasing with mass flow, as expected. Increase of the secondary electron emission coefficient is decreasing the energy and increasing the ion flow. It is quite expected as well: an increased source of electrons will result in an increased plasma flow and divide the available energy over more particles. The effect on energy is only a slight decrease but the increase on ion flow is more significant. Thus increase in secondary electron emission results in an increased thrust (since thrust is proportional to ion flow and to the square root of the ion energy).

DOI: 10.13009/EUCASS2019-967

	P_{in} (W)	ψ_g (mg/s)	γ	Ion energy (eV)	Ion flow (fraction of gas flow)
Case 1	10	0.1	1.8	190	0.65
Case 2	20	0.1	1.8	325	0.77
Case 3	50	0.1	1.8	700	0.88
Case 4	20	0.08	1.8	350	0.85
Case 5	20	0.2	1.8	190	0.65
Case 6	20	0.4	1.8	120	0.52
Case 7	20	0.1	1.4	335	0.7
Case 8	20	0.1	2.2	320	0.81

Table 1 : Parametric study

Although the results are only preliminary, a first comparison between the results of the model and experimental data is provided on Figure 6 and Figure 7. Figure 6 displays the ion average energy as a function of input energy in eV per injected atom of neutral xenon. The model predicts a linear increasing trend. Measurements show an increasing trend as well but with lower ion energy, and increasing slope. The offset between the experimental and calculated data could be explained by the fact that background tank pressure is a parameter that is ignored by the modelling. Yet, it is a well-known experimental fact that for this thruster that a higher xenon pumping speed allows significantly higher ion energy [14]. An increased xenon pumping speed would therefore bring the experimental data closer to the results of this modelling.

On Figure 7 the mass utilization efficiency (i.e. ion flow as a fraction of gas flow) is plotted as a function of input energy in eV per injected atom of neutral xenon. The model predicts a similar trend but significantly off-set to higher values than that experimentally measured. This may invite to consider additional loss mechanisms in the model, in particular: Coulomb elastic scattering and anomalous cross-field mobility.

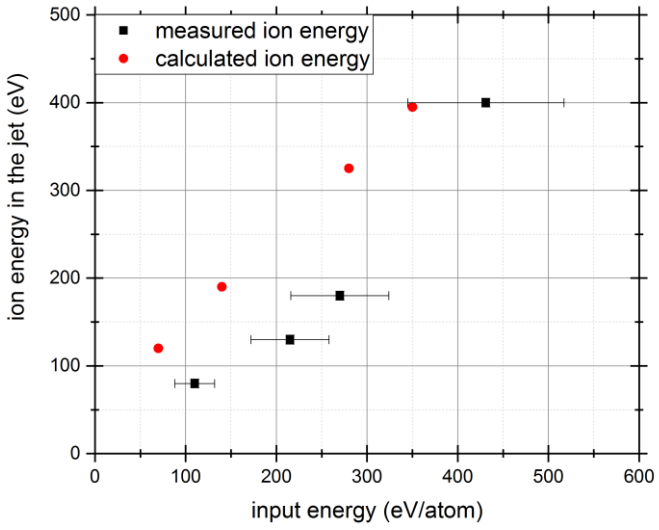

Figure 6 : Ion energy as a function of input energy. In red: calculated by the model for γ = 1.8. In black: measured. From [15], with a corrective factor for microwave losses that were apparently not accounted for

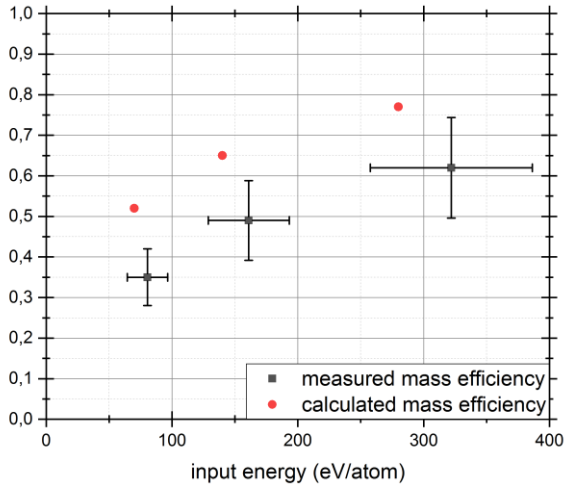

Figure 7 : Mass utilization efficiency as a function of input energy. In red: calculated by the model for γ = 1.8 and P_{in} = 20W. In black: measured around 23W. From [15], with a corrective factor for microwave losses that were apparently not accounted for

4 Conclusion

A quasi linear heating model for an ECR plasma thruster has been presented as well as preliminary results compared with experimental data. It is a satisfaction to provide a model, however simple, that is taking into account the kinetic nature of the heating process occurring in the thruster. The model points out the influence of the secondary electron emission at the backplate, a parameter that might have been previously overlooked. The comparison with experimental data is encouraging given the simplicity of the model and the fact that the dramatic effect of the xenon background tank pressure is not modelled. If the discrepancy between the experimental and calculated data were confirmed after addressing the background tank pressure effect, it may invite to reconsider the derivation of the diffusion coefficient.

The derivation of the diffusion coefficient is indeed a difficult issue that will require further work. It could also be fitted to test the validly of the rest of model against experimental data. Additional loss mechanisms such as anomalous cross-field mobility and Coulomb scattering could also be considered. The calculation of the distribution function in z is also part of the work plan. This would provide insight on the axial dynamics of the thruster such as the distribution of ionization along the axis of the thruster.

References

[1] T. Wekerle *et al.*, 'Status and Trends of Smallsats and Their Launch Vehicles — An Up-to-date Review', *J. Aerosp. Technol. Manag.*, vol. 9, no. 3, pp. 269–286, Sep. 2017.

[2] D. Packan *et al.*, 'The "MINOTOR" H2020 project for ECR thruster development', in *35th International Electric Propulsion Conference, No. IEPC-2017-547, Electric Rocket Propulsion Society, Fairview Park, OH*, 2017.

[3] F. Cannat, T. Lafleur, J. Jarrige, P. Chabert, P.-Q. Elias, and D. Packan, 'Optimization of a coaxial electron cyclotron resonance plasma thruster with an analytical model', *Phys. Plasmas*, vol. 22, no. 5, p. 053503, May 2015.

[4] T. Vialis, J. Jarrige, A. Aanesland, and D. Packan, 'Direct Thrust Measurement of an Electron Cyclotron Resonance Plasma Thruster', *J. Propuls. Power*, vol. 34, no. 5, pp. 1323–1333, 2018.

DOI: 10.13009/EUCASS2019-967

[5] P.-Q. Elias, 'Advances in the kinetic simulation of the microwave absorption in an ECR thruster', presented at the IEPC, 2017.
[6] E. Ahedo and M. Merino, 'Two-dimensional supersonic plasma acceleration in a magnetic nozzle', *Phys. Plasmas*, vol. 17, no. 7, p. 073501, Jul. 2010.
[7] M. Martinez-Sanchez, J. Navarro-Cavallé, and E. Ahedo, 'Electron cooling and finite potential drop in a magnetized plasma expansion', *Phys. Plasmas*, vol. 22, no. 5, p. 053501, May 2015.
[8] J. A. Bittencourt, *Fundamentals of Plasma Physics*. Springer Science & Business Media, 2004.
[9] J. Jarrige, S. Correyero Plaza, P.-Q. Elias, and D. Packan, 'Investigation on the ion velocity distribution in the magnetic nozzle of an ECR plasma thruster using LIF measurements', presented at the IEPC, 2017.
[10] J.-M. Rax, *Physique des plasmas - Cours et applications*. Paris: Dunod, 2005.
[11] M. A. Lieberman and A. J. Lichtenberg, 'Theory of electron cyclotron resonance heating. II. Long time and stochastic effects', *Plasma Phys.*, vol. 15, no. 2, pp. 125–150, Feb. 1973.
[12] Marc Villemant, 'Modélisation et caractérisation expérimentale de l'influence de l'emission électronique sur le fonctionnement des propulseurs à courant de Hall', ISAE, 2018.
[13] J. Meunier, Ph. Belenguer, and J. P. Boeuf, 'Numerical model of an ac plasma display panel cell in neon-xenon mixtures', *J. Appl. Phys.*, vol. 78, no. 2, pp. 731–745, Jul. 1995.
[14] T. Vialis, 'Développement d'un propulseur plasma à résonance cyclotron électronique pour les satellites', 2018.
[15] F. Cannat, 'Caractérisation et modélisation d'un propulseur plasma à résonance cyclotronique des électrons', phdthesis, Ecole doctorale de l'Ecole Polytechnique, 2015.